Journal of
Ceramic Science
and Technology

J. Ceram. Sci. Technol., **09** [1] 1-6 (2018)
DOI: 10.4416/JCST2017-00044
available online at: http://www.ceramic-science.com

Microstructure and Phase Evolution of Cement-Bonded High-Alumina Refractory Castables for Porous Purging Plugs

Q. Wang[1], Y. Li[*1], N. Xu[1], R. Xiang[1], S. Li[1]

[1]The State Key Laboratory of Refractories and Metallurgy, Wuhan University of Science and Technology (WUST), Wuhan 430081, China

received June 25, 2017; received in revised form August 15, 2017; accepted September 6, 2017

Abstract

This work addresses the microstructure and phase evolution of four designed high-alumina refractory castables (containing ϱ-Al_2O_3 or calcium aluminate cement as a binder source and 0 or 1 wt% microsilica). Various experimental tests (air permeability, linear change rate, apparent porosity, cold modulus of rupture, cold crushing strength, hot modulus of rupture, pore size distribution, X-ray diffraction and scanning electron microscopy) were conducted to characterize the castables. The results show that using cement as the binder has a significant effect on the properties of the refractory castables. The cement-bonded castables exhibited a lower linear shrinkage rate, apparent porosity and air permeability, higher cold modulus of rupture and cold crushing strength, as well as a smaller mean pore size than that of the ϱ-Al_2O_3-bonded castables. The results were attributed to the formation of calcium hexaluminate. Some CA_6 was detected inside the pores, which occupied space in the pores and prevented the formation of interconnected pores, while some CA_6 existed outside the pores, which enhanced the densification of the structure and reduced the size of pores. Moreover, the addition of microsilica can facilitate interconnected pore formation in cement-bonded castables, but lower the hot modulus of rupture owing to the formation of low-melting-temperature phase (C_2AS).

Keywords: Cement, porous purging plug, microstructure, phase evolution, pore size distribution

I. Introduction

A purging plug is an important functional component with purpose of accelerating physical and chemical reactions in a steel ladle, homogenizing the temperature and composition of steel, facilitating the floating of impurities during steel refining. Two types of purging plug have been commonly used over the past few decades; a porous-type plug and slit-type plug [1]. The porous-type plug exhibits excellent bubbling reliability [2] and is more effective in removing impurities from molten steel than the slit-type plug. Interconnected pores are a crucial factor in its structure.

Thanks to their high refractoriness, slag resistance and high chemical stability, high-alumina castables are widely used in high-temperature industries, such as metallurgy, building materials, petrochemicals and so on [3]. Calcium aluminate cement (CAC) and ϱ-Al_2O_3 are common binders in refractory castables. But ϱ-Al_2O_3-bonded castables exhibit structural spalling [4], resulting from a characteristic drop in strength at intermediate temperatures (110 – 1000 °C) [5–7] during the decomposition of hydrates.

Microsilica is another important component usually found in the matrix composition of castables. Composed of sub-micrometric amorphous SiO_2 particles and particles of spherical shape [8,9], its role is mostly related to improving flowability in order to enhance workability.

With regard to these aspects, this work addresses the microstructure and phase evolution of four designed high-alumina refractory castables (containing ϱ-Al_2O_3 or CAC as a binder source and 0 or 1 wt% microsilica). Various experimental tests (air permeability, linear change rate, apparent porosity, pore size distribution, cold modulus of rupture (CMOR), cold crushing strength (CCS), hot modulus of rupture (HMOR), X-ray diffraction (XRD) and scanning electron microscopy (SEM)) were conducted to characterize the castables and confirmed the effect of cement on the microstructure and phase composition of high-alumina refractory castables.

II. Experimental

(1) Sample preparation

Tabular alumina (3 – 1 mm, 98 wt% Al_2O_3, Zhejiang Zilialumina Material Technology Co., Ltd. China), reactive alumina powder (CL370, Almatis, USA) and $Al(OH)_3$ (Chalco Shandong Advanced Material Co., Ltd. China) were used as the main raw materials. ADS1 and ADW1 (Almatis, USA) were used as dispersants. In addition, calcium aluminate cement (Secar 71, Kerneos, France) and ϱ-Al_2O_3 (5 μm, 85 % Al_2O_3, Kaifeng Special Refractories Co., Ltd., China) were used as the binders in different castables. Different amounts of microsilica (0.5 μm, 951UL, Elkem, Norway) were added to the samples. The detailed formulations are provided in Table 1. The raw ma-

* Corresponding author: lybref2002@126.com

terials were cast in a castable mixer by dry mixing for 1 min, followed by the addition of water and dispersant. After another 4 min of mixing, the mixture was vibrocast into 160 mm × 40 mm × 40 mm cuboid molds and 50 mm × 50 mm circular cylinder molds. All samples were cured at room temperature for 24 h and subsequently dried at 110 °C for another 24 h. Finally, the samples were calcined at 1100 °C, and 1550 °C respectively, with a heating rate of 3 K/min and a holding time of 3 h before they were allowed to cool to room temperature.

Table 1: Detailed high-alumina castable formulations.

Composition (wt%)	Particle size	A	B	C	D
Tabular alumina	1 – 3 mm	71	71	71	71
CL370	2 μm	13	13	13	13
$Al(OH)_3$	0.088 mm	12	12	12	12
Secar71	–	5	5	–	–
ϱ-Al_2O_3	5 μm	–	–	5	5
Microsilica	0.5 μm	–	1	–	1
ADS1	–	0.5	0.5	0.5	0.5
ADW1	–	0.5	0.5	0.5	0.5

(2) Test and characterization methods

The linear change rate was determined based on length measurements before and after the sintering process. The apparent porosity (AP) was tested according to the Archimedes principle. The cold modulus of rupture (CMOR) was determined in a three-point bending test at ambient temperature, and the cold crushing strength (CCS) was evaluated in a hydraulic testing machine. The hot modulus of rupture (HMOR) was measured in a three-point bending test at 1400 °C for a soaking time of 0.5 h with an electronic digital control system (EDC120; DOLIC company, Germany). The air permeability was obtained in compliance with the Chinese standard GB/T 3000 – 1999. The pore size distribution was examined by means of mercury intrusion porosimetry (Quantachrome PM60GT-18, Quantachrome Instruments Ltd., USA). The phase composition and microstructure were analyzed using X-ray diffraction (XRD, X'Pert Pro) and field emission scanning electron microscopy (SEM, Nova 400 Nano) supported by energy-dispersive X-ray spectroscopy (EDS, Phoenix).

III. Results and Discussions

Fig. 1 shows XRD patterns of samples A, B, C and D after these had been calcined at (a) 1100 °C and (b) 1550 °C. As shown, the main crystalline phase of the four samples was Al_2O_3. For samples A and B, after these had been calcined at 1100 °C, traces of CA_2 were detected, but the peak intensities of this phase for sample A are much higher compared with those of sample B. Usually, the CA phase existing in calcium alumina cement reacts with alumina to form CA_2 [10] in the 1000 – 1200 °C range [11 – 13]. After calcining at 1550 °C, a large amount of CA_6 was formed, especially in the case of sample A. Generally, CA_6 formation takes place above 1400 °C [6, 7, 14]. Increasing the calcination temperature facilitated the formation of CA_6. For sample B, traces of C_2AS were formed owing to the addition of microsilica [15 – 19].

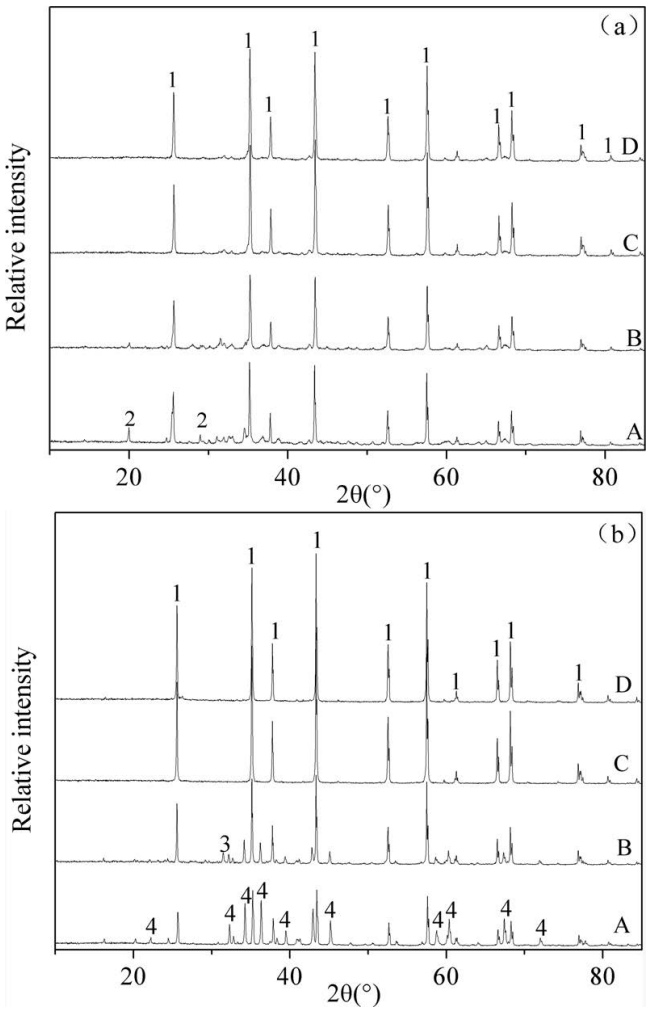

Fig. 1: XRD patterns of samples A, B, C and D after these had been calcined at (a) 1100 °C and (b) 1550 °C, 1, Al_2O_3; 2, CA_2; 3, C_2AS; 4, CA_6.

Fig. 2 presents the linear change rate of the high-alumina castables containing different binders. The four samples showed different shrinkage after being calcined at 1100 °C and 1550 °C. After being calcined at 1100 °C, the cement-bonded castables exhibited lower shrinkage because of the expansion resulting from the formation of CA_2 [20, 21] (Fig. 1(a)), which counterbalanced the sintering shrinkage. When microsilica was added, the samples showed higher shrinkage. The first reason was that the presence of microsilica facilitates liquid formation, which helped the sintering process. The second reason was that some Ca^{2+} entered the liquid, which reduced the CA_2 content and lowered the expansion. Because of these two reasons, sample B exhibited higher shrinkage than that of sample A. When calcined at 1550 °C, owing to the sintering shrinkage, all samples exhibited higher shrinkage compared to that of the samples calcined at 1100 °C. However, sample A exhibited the lowest shrinkage owing to

CA_6 formation (Fig. 1(b)). But the shrinkage of the sample with the addition of 1 % microsilica (sample B) is similar to that of the sample without cement (sample C). The low-melting-temperature phase (C_2AS) formation [15–19] counterbalanced the expansion resulting from the CA_6 formation [10].

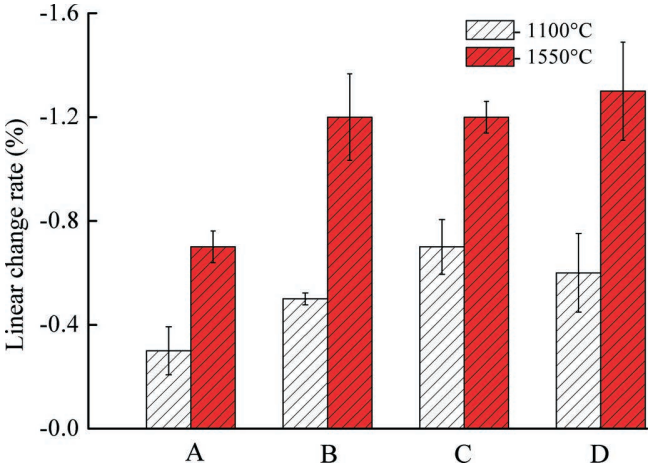

Fig. 2: Linear change rate of the samples after these had been calcined at 1100 °C and 1550 °C.

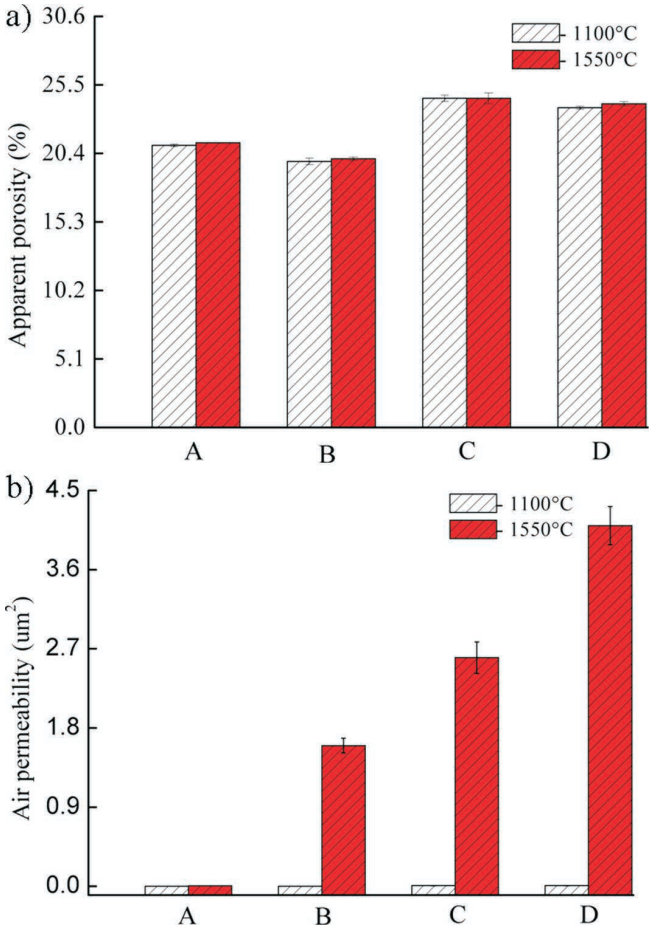

Fig. 3: Apparent porosity and air permeability of the samples after these had been calcined at 1100 °C and 1550 °C.

Apparent porosity and air permeability were determined for the samples prepared at 1100 °C and 1550 °C. Fig. 3(a) shows that the cement-bonded samples have lower apparent porosity compared with that of the ϱ-Al_2O_3-bonded samples. Owing to the expansion phase (CA_2 at 1100 °C and CA_6 at 1550 °C) formation, some space in samples was filled and the structure became denser. Fig. 3(b) shows the air permeability was different. After being calcined at 1100 °C, the four samples had almost no air permeability, which was attributed to the absence of sintering. Air permeability was clearly enhanced after calcining at 1550 °C owing to the sintering process. But the cement-bonded samples exhibited lower air permeability. One reason is that the samples had lower apparent porosity and the other reason is attributed to the formation of CA_6, which occupied some space and prevented pores linking up. Compared with sample A, sample B exhibited higher air permeability owing to the addition of microsilica. During the calcining process, SiO_2 reacted with Al_2O_3 and CaO to form liquid, which counterbalanced the expansion. And the reaction consumed some CaO, which reduced the quantity of CA_6 phase formed.

The mean pore size and pore size distribution of samples A, B, C and D after these had been calcined at 1550 °C are shown in Fig. 4. It can be observed from Fig. 4(a) that sample A possessed the smallest mean pore size and microsilica addition facilitated the increase in pore size. For cement-bonded castables, the mean pore size changed from 0.92 μm to 13.77 μm, while for ϱ-Al_2O_3-bonded castables, it increased from 6.09 μm to 10.10 μm. From Fig. 4(b), it can be seen that sample A had the narrowest pore size distribution and bigger pores cannot be found compared with other samples.

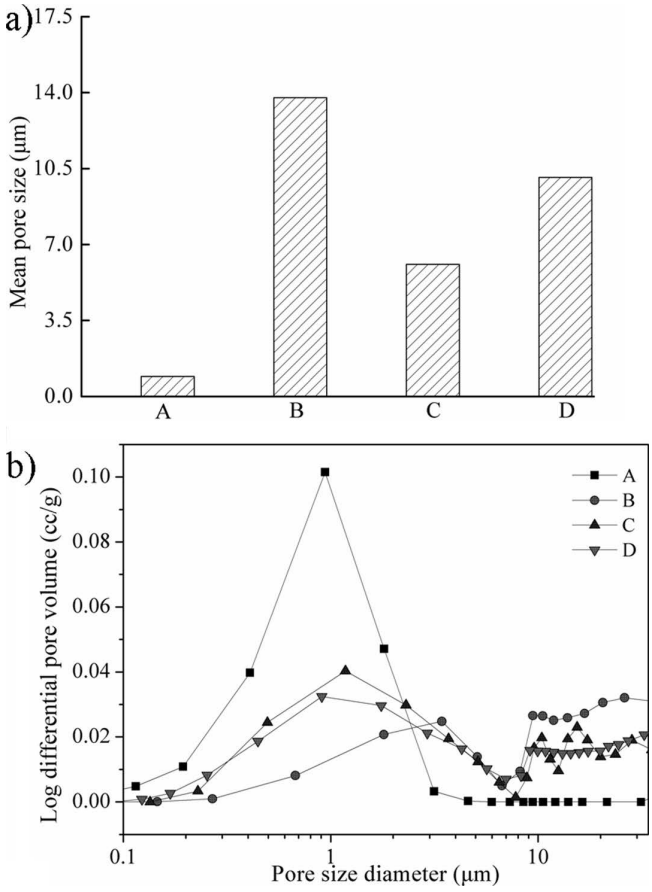

Fig. 4: Mean pore size and pore size distribution of samples A, B, C and D after these had been calcined at 1550 °C.

Fig. 5 shows the SEM images for samples A, B, C and D after they had been calcined at 1550 °C for 3 h. From the images, we can see the structure is different from the dense structure. The dense structure can be defined in that coarser particles are used as a filter framework and smaller particles fill the voids between the coarser particles, but this work presents the idea that larger particles are used as the framework and smaller particles are removed, leaving behind many pores capable of forming interconnected pores [22]. But in Fig. 5(A) the structure is very dense and the pores are smaller and isolated while in the other samples some bigger pores and cracks existed in the samples, which facilitated the formation of interconnected pores. The smaller pores came from thermal decomposition of the $Al(OH)_3$, but the morphology of $Al(OH)_3$ remained. Li *et al.* [23] called them "pseudomorph", which can be seen from the magnifying micrograph of sample A (Fig. 6a). The formation of the bigger pores in Fig. 5 (B, C, D) was attributed to particle packing of aggregate and volumetric shrinkage of the matrix, while the microstructure of sample A appears denser owing to the expansion of CA_6. The microstructure is in line with the results of pore size distribution (Fig. 4(b)). Fig. 6(b) shows a magnified micrograph of sample A and CA_6 phase can be detected. From the image, we can see that the CA_6 was flake-like. Some existed inside the pores, occupying some space in the pores and preventing the formation of interconnected pores while some was outside the pores, which enhanced the densification of sample and reduced the size of pores owing to the expansion of CA_6.

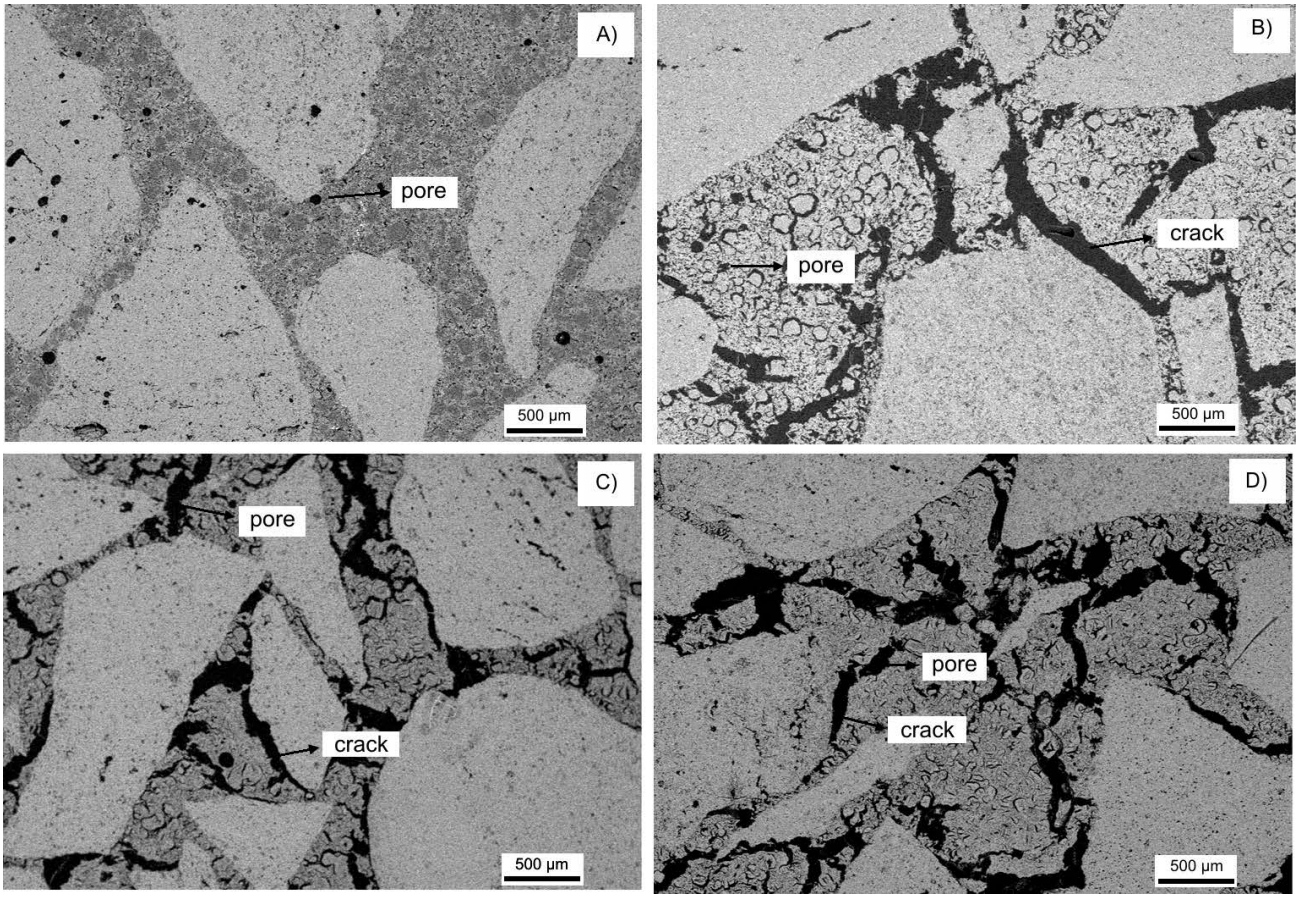

Fig. 5: SEM images of samples A, B, C and D after these had been calcined at 1550 °C.

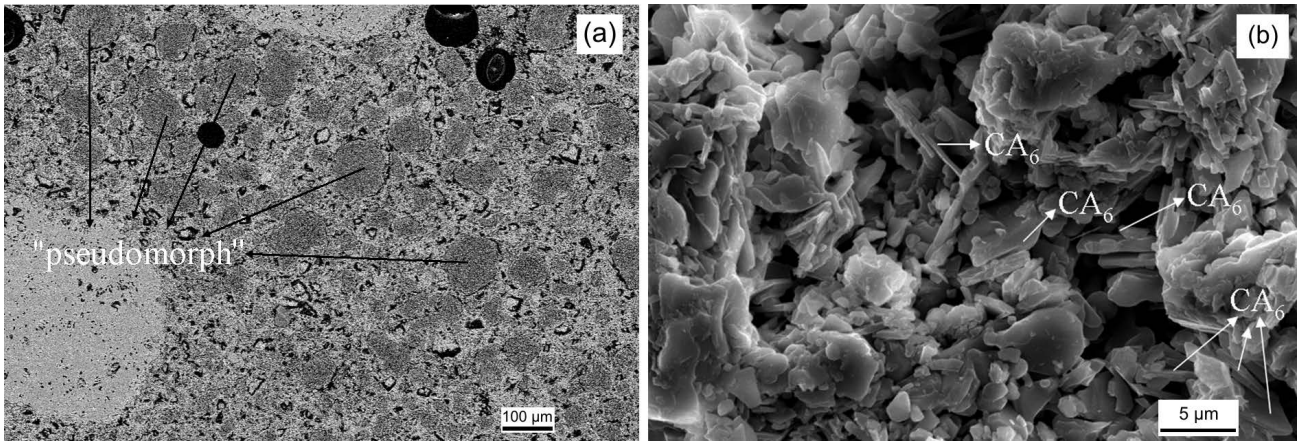

Fig. 6: SEM micrograph of sample A after this had been calcined at 1550 °C.

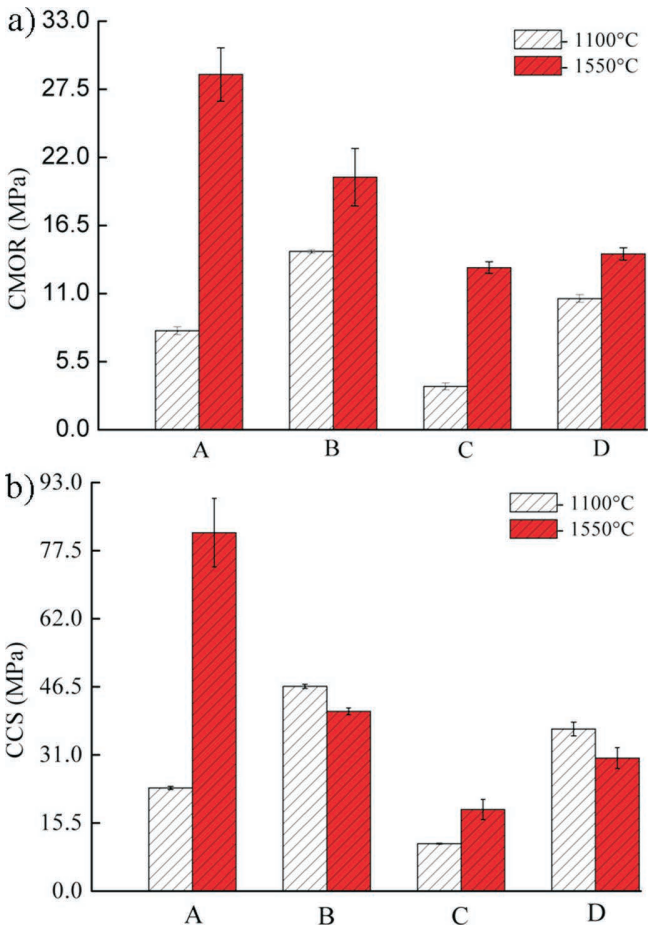

Fig. 7: CMOR and CCS of the samples after these had been calcined at 1100 °C and 1550 °C.

Fig. 7 shows that the CMOR and CCS of samples A, B, C and D have the same changed tendency. After being calcined at 1100 °C, the samples with added microsilica exhibited higher strength than those without microsilica. And the cement-bonded castables possessed higher strength than that of the ϱ-Al_2O_3-bonded castables. And after calcining at 1550 °C, the addition of microsilica reduced the strength of the cement-bonded samples but increased the strength of the ϱ-Al_2O_3-bonded samples. And the strength of the cement-bonded castables is higher than that of the ϱ-Al_2O_3-bonded castables. The results were associated with both the pore size and apparent porosity. Generally, the smaller the pore size is, the higher the strength will be; and the higher the apparent porosity is, the lower the strength will be. Rice proposed a simple relationship used to reflect the strength (σ)-porosity (P) behaviors [24]. The relation is:

$$\sigma=\sigma_0 \exp(-b P)$$

where σ_0 is the strength of the samples without pores, and b is a constant associated with the pore characteristics. From this relation, it can be seen that the strength decreased with the increase in porosity. From Fig. 3(a), after calcining at 1550 °C, the apparent porosity is: B<A<D<C, while from Fig. 7(a) the strength is: A>B>D>C. The results are not completely in line with the relation. Because strength is not only associated with the apparent porosity, but also with the pore size. As shown in Fig. 4, sample A exhibited many smaller pores, fewer bigger pores and the mean pore size is 0.92 μm while the pore size of the sample B is bigger and the mean pore size is 13.77 μm. The smaller pores contributed to the improvement of strength, and the strength of sample A is higher than that of sample B even though the apparent porosity of sample A is higher.

As shown in Fig. 8, the HMOR of sample A is the highest of samples A, B, C and D. It can reach 14.6 MPa. And that of samples B, C and D is less than 2 MPa. The apparent porosity of samples C and D is higher than that of sample A. It is easy to understand that the HMOR is lower than that of sample A. For sample B, the low-melting-temperature phase (C_2AS) formation [15–19] seriously reduced the HMOR [25].

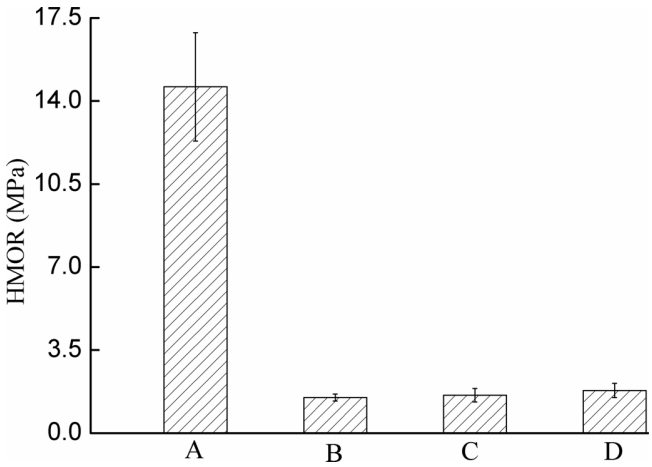

Fig. 8: HMOR of samples with different binders.

IV. Conclusions

The attained results show that cement as the binder has a significant effect on the properties of the high-alumina refractory castables. The cement-bonded castables exhibited a lower linear shrinkage rate, apparent porosity and air permeability, higher CMOR and CCS, and smaller mean pore size than that of the ϱ-Al_2O_3-bonded castables. The results were attributed to the formation of calcium hexaluminate (CA_6). Some CA_6 was detected inside the pores; it occupied some space in the pores and prevented the formation of interconnected pores. Some CA_6 existed outside the pores, which enhanced densification of the samples and, because of the expansion of CA_6, reduced the size of pores. Moreover, the addition of microsilica can facilitate interconnected pore formation in cement-bonded castables. but lowers the hot modulus of rupture owing to the formation of low-melting-temperature phase (C_2AS).

Acknowledgements

This work was supported by the National Natural Science Foundation of China (51502213) and the State Key Laboratory Project Fund (G201507).

References

1 Primachenko, V.V., Martynenko, V.V., Ustichenko, V.A.: The manufacturing experience and an application in the Ukraine mullite-corundum purging plugs for the blowing of steel in the ladles. In: Proceedings of UNITECR'01. Cancun, Mexico, 2001.

[2] Kimura, M., Ohuchi, T., Tsuzuki, T., *et al.*: Development and application of porous type gas purging plug with high bubbling reliability and durability. In: Proceedings of UNITECR'01, Cancun, Mexico, 2001.

[3] Li, Z.G., Ye, F.B., Zhang, Y.: Effects of nano calcium carbonate on strength and microstructure of Corundum-based castables, *China Refract.*, **19**, 1 – 6, (2010).

[4] Auvray, J.M., Gault, C., Huger, M.: Evolution of elastic properties and microstructural changes versus temperature in bonding phases of alumina and alumina-magnesia refractory castables, *J. Eur. Ceram. Soc.*, **27**, 3489 – 3496, (2007).

[5] Braulio, M.A.L., Milanez, D.H., Sako, E.Y., Bittencourt, L.R.M., Pandolfelli, V.C.: Expansion behavior of cement bonded alumina-magnesia refractory castables, *Am. Ceram. Soc. Bull.*, **86**, 9201 – 9206, (2007).

[6] Ide, K., Suzuki, T., Asano, K., Nishi, T., Isobe, T., Ichikawa, H.: Expansion behavior of alumina-magnesia castables, *J. Tech. Assoc. Refract.*, **25**, 202 – 208, (2005).

[7] Ko, Y.C., Lay, J.T.: Thermal expansion characteristics of alumina-magnesia and alumina-spinel castables in the temperature range 800°– 1650 °C, *J. Am. Ceram. Soc.*, **83**, 2872 – 74, (2000).

[8] Myhre, B.: Microsilica in refractory castables – how does microsilica quality influence performance? In: Proceedings of Unified International Conference on Refractories, Orlando, USA, 191 – 195, (2005).

[9] Liu, G., Jin, X., Qiu. W., *et al.*: The effect of microsilica on the oxidation resistance of Al_2O_3-SiC-SiO_2-C castables with Si and B_4C additives, *Ceram. Int.*, **42**, 251 – 262, (2016).

[10] Wang, Q., Ye, G., Wang, Y., *et al.*: Effect of micro-sized calcium carbonate addition on volumetric stability and strength of corundum-based castables, *Int. J. Appl. Ceram. Technol.*, **12**, E166 – E171, (2015).

[11] Auvray, J.M., Gault, C., Huger, M.: Microstructural changes and evolutions of elastic properties versus temperature of alumina and alumina-magnesia refractory castables, *J. Eur. Ceram. Soc.*, **28**, 1953 – 1960, (2008).

[12] Fuhrer, M., Hey, A., Lee, W.E.: Microstructural evolution in self-forming spinel/calcium aluminate-bonded castable refractories, *J. Eur. Ceram. Soc.*, **18**, 813 – 820, (1998).

[13] Díaz, L.A., Torrecillas, R.: Hot bending strength and creep behavior at 1000 – 1400 °C of high alumina refractory castables with spinel, periclase and dolomite additions, *J. Eur. Ceram. Soc.*, **29**, 53 – 58, (2009).

[14] Wang, Y., Li, X., Zhu, B., *et al.*: Microstructure evolution during the heating process and its effect on the elastic properties of CAC-bonded alumina castables, *Ceram. Int.*, **42**, 11355 – 11362, (2016).

[15] Lee, W.E., Vieira, W., Zhang, S., Ahari, K.G., Sarpoolaky, H., Parr, C.: Castable refractory concretes, *Int. Mater. Rev.*, **46**, 145 – 167, (2001).

[16] Braulio, M.A.L., *et al.*: Microsilica effects on cement bonded alumina-magnesia refractory castables, *Refract.*, **62**, 543 – 549, (2010).

[17] Sandberg, B., Myhre, B.: Castables in the System MgO-$A1_2O_3$-SiO_2. In: Proceedings of UNITECR'95, Kyoto, Japan, 1995.

[18] Braulio, M.A.L., Rigaud, M., Buhr, A., Parr, C., Pandolfelli, V.C.: Spinel-containing alumina-based refractory castables, *Ceram. Int.*, **37**, 1705 – 1724, (2011).

[19] Zhang, S., Lee, W. E.: Refractories Handbook. Marcel Dekker lnc., USA., 2004.

[20] Criado, E., Estrada, D.A., DeAza, S.: Dilatometric study of the formation of CA_2 and CA_6 in cements and refractory concretes, *Bull. Span. Ceram. Glass Soc.*, **15**, 319 – 321, (1976).

[21] Criado, E., Caballero, A., Pena, P.: Microstructural and mechanical properties of alumina-calcium hexaluminate composites. In: The World Congress on High Tech Ceramics. Milan, Italy, 1986.

[22] Wang, Q.H., Li, Y.B., Li, S.J. *et al.*: Effects of critical particle size on properties and microstructure of porous purging materials, *Mater. Lett.*, **197**, 48 – 51, (2017).

[23] Li, S., Li, N.: Effects of composition and temperature on porosity and pore size distribution of porous ceramics prepared from $Al(OH)_3$, and kaolinite gangue, *Ceram. Int.*, **33**, 551 – 556, (2007).

[24] Rice, R.W.: Comparison of stress concentration versus minimum solid area based mechanical property-porosity relations, *J. Mater. Sci.*, **28**, 2187 – 2190, (1993).

[25] Souza, T.M., Luz, A.P., Brito, M.A.M. *et al.*: In situ elastic modulus evaluation of Al_2O_3-MgO refractory castables, *Ceram. Int.*, **40**, 1699 – 1707, (2014).